Observations of Radar Backscatter at Ku and C Bands in the Presence of Large Waves during the Surface Wave Dynamics Experiment

S. V. Nghiem, *Member, IEEE*, Fuk K. Li, *Senior Member, IEEE*, Shu-hsiang Lou, Gregory Neumann, Robert E. McIntosh, *Fellow, IEEE*, Steven C. Carson, James R. Carswell, Edward J. Walsh, *Member, IEEE*, Mark A. Donelan, and William M. Drennan

Abstract— **Ocean radar backscatter in the presence of large waves is investigated using data acquired with the Jet Propulsion Laboratory NUSCAT radar at Ku band for horizontal and vertical polarizations and the University of Massachusetts C-SCAT radar at C band for vertical polarization during the Surface Wave Dynamics Experiment. Off-nadir backscatter data of ocean surfaces were obtained in the presence of large waves with significant wave height up to 5.6 m. In moderate-wind cases, effects of large waves are not detectable within the measurement uncertainty and no noticeable correlation between backscatter coefficients and wave height is found. Under high-wave light-wind conditions, backscatter is enhanced significantly at large incidence angles with a weaker effect at small incidence angles. Backscatter coefficients in the wind speed range under consideration are compared with SASS-II (Ku band), CMOD3-H1 (C band), and Plant's model results which confirm the experimental observations. Variations of the friction velocity, which can give rise to the observed backscatter behaviors in the presence of large waves, are presented.**

I. Introduction

RADAR scatterometry is a technique for remote sensing of the near surface wind speed and direction over the ocean. Sensors have been successfully developed and flown at Ku band on the SEASAT [1] satellite in 1978, and at C band on the operational ERS-1 satellite [2]. The small scale ocean surface roughness increases with increasing local winds, and this increased roughness enhances the off-nadir radar cross section of the ocean. This indirect relationship forms the basis of using radar scatterometry for ocean wind measurements. The relationship can be modified when waves with large significant wave heights (SWH), caused by strong winds earlier or by swells propagating into the local area, are present. In this case, the accuracy of radar scatterometry in retrieving the ocean surface wind field can be affected by the presence of such large waves.

The effects of high waves on ocean radar backscatter have been investigated with theoretical models. Based upon a model for a wind-driven sea with swells, [3] predicted that a very large amplitude swell can significantly increase the backscatter coefficients at low radar frequency (L band), small incidence angle and light wind; however, the predicted effects will be small at Ku band and large incidence angles for all wind speeds. Reference [4] indicated that a swell traveling at a large angle oblique to the wind direction can have an important impact on scatterometry. This is the case especially for light wind and low incidence angles because the backscatter extrema are not necessarily in the local wind direction. At larger incidence angles, this model suggests that the large-wave effects diminish because the contribution of specular backscatter becomes less important as compared to the Bragg contribution for the short wave part of the composite spectrum. References [5], [6] applied the principle of the conservation of wave action to modeling the interactions between long and short waves on the water surface by using a hydrodynamic modulation transfer function. This model indicates that the long-wave properties can also affect the normalized radar cross section of the ocean through the second-order effects of short-wave tilting and hydrodynamic modulation. In the calculation of backscatter coefficients in this model, however, the long and short waves are assumed to be local wind generated, and therefore the direction of these waves are aligned.

Experimentally, tower based measurements at L- and Ku-band frequencies [7] have been made to study the radar dependence upon ocean waves. Horizontally polarized backscatter data at L band were taken at incidence angles of 35° and 45°, and azimuthal angles from 225° through North to 60°. Vertically polarized Ku-band data were collected only at 45° incidence angle, with azimuthal angles limited to 300°–360°. Most of the long waves encountered during this experiment were not generated by the local wind. At lower wind speeds, these measurements suggest that radar cross sections may be slightly lowered when long waves propagate at a large angle to the wind. At the C band frequency of 5.3 GHz, airborne

Manuscript received March 3, 1994; revised October 11, 1994. This research was carried out by the Jet Propulsion Laboratory, California Institute of Technology, under a contract with the National Aeronautics and Space Administration. This work was supported in part by the Office of Naval Research under Grant N00014-88-J-1028.

S. V. Nghiem, F. K. Li, S. H. Lou, and G. Neumann are with the Jet Propulsion Laboratory, California Institute of Technology, Pasadena, CA 91109 USA.

R. E. McIntosh, S. C. Carson, and J. R. Carswell are with the Department of Electrical Engineering, University of Massachusetts, Amherst, MA 01003 USA.

E. J. Walsh is with the NASA Goddard Space Flight Center, Observational *Science Branch*, Laboratory for Hydrospheric Processes, Wallops Flight Facility, Wallops Island, VA. He is presently on assignment at R/E/ET6, NOAA Environmental Technology Laboratory, Boulder, CO 80303 USA.

M. A. Donelan and W. M. Drennan are with the National Water Research Institute, Burlington, ON, Canada.

IEEE Log Number 9411230.

measurements [8] were obtained for radar cross section as a function of wind speed. The data seem to indicate that the upwind/crosswind ratio is the largest when the wind blows in the wave direction. The implications of these experiments are tentative and need further data for their confirmation.

This paper presents a case study of radar backscatter from the ocean surface at Ku and C bands in the presence of large waves. The data were acquired during the Surface Wave Dynamics Experiment (SWADE) in 1991 when two airborne scatterometers were flown together on the NASA Ames C130B aircraft: NUSCAT, a Ku-band scatterometer developed at the Jet Propulsion Laboratory (JPL), and C-SCAT, a C-band scatterometer developed at the University of Massachusetts (UMass). The plane flew over an instrumented oceanic area off the U.S. East coast near 37° North latitude and 74° West longitude. Backscatter coefficients obtained on Mar. 4, 1991 in the presence of swells with SWH as high as 5.6 m are compared with data at lower SWH under similar wind conditions. Wind speeds were in both moderate and light wind ranges. Although the observations were limited to a narrow set of conditions, they represent a quantitative evaluation of the variation in the radar cross section in the presence of large waves at two different radar frequencies. In addition, several buoys measured atmospheric and oceanic parameters, another airborne radar acquired directional wave spectra, and a ship was deployed to make measurements including friction velocities. The backscatter measurements are also compared with calculations from empirical and theoretical models.

Section II below shows the data sets selected for this study and the results for observations of radar backscatter in the presence of large waves and Section III compares the experimental measurements with model results. The appendix describes in details the NUSCAT and C-SCAT scatterometers, the SWADE location, the experimental scenario, the directional wave fields, and sea surface temperature effects.

II. Radar Observations in the Presence of Large Waves

A. Data Selection

A specific scatterometer data set was chosen from the SWADE data base in which the SWH was high and was compared with data sets taken at lower SWH to evaluate the effects of large waves. The criteria for the data selection were: 1) the measurements had the same polarization and incidence angle, 2) the wind speeds for these cases were close ($\lesssim$ 1 $\mathrm{M \cdot s^{-1}}$ difference), 3) the backscatter data were collected at the location nearest to the buoy in question, and 4) Gulf Stream boundary crossings with potential complications in the ocean conditions were avoided. These criteria were chosen to isolate cases with high and low SWH while the other scatterometer and oceanic parameters were as similar as possible. As Table VI and Figs. 14 and 15 in the appendix show, large significant wave heights occurred predominantly during flight 5 on Mar. 4, 1991. Data sets collected under high SWH conditions were selected first, and then corresponding cases with low SWH were chosen using the criteria listed above. Table VI indicates that the ocean conditions measured by the buoys at different locations can be quite different. This suggests that the winds were very inhomogeneous spatially. This was especially true of the data collected at buoy A, where several cases of light to very low winds were observed. Since this buoy was in the cold, shallow, near shore waters where the ocean conditions were quite different from the other buoys, none of these data was used. In general, the low SWH cases used for comparison came from flight 9 for moderate wind speed cases, and flight 6 for low wind speed cases. For most of the cases, radar data selected for the analysis in this paper were collected along flight lines over buoy positions. During the time of a radar data take (approximately 3 minutes), the aircraft moved about 20 km; therefore, the radar data were within 20 km around the buoys. Only in the case of 50° incidence angle at horizontal polarization for light wind and high wave conditions, the closest location of the radar data was 50 km away from the buoy.

The wind speeds for the high and low SWH cases were, in general, not exactly the same, and since the normalized radar cross section of the ocean is strongly dependent upon the wind, a scheme was developed to account for the wind difference. Consider a case with low SWH where the wind speed is close but not the same as the wind in a case with high SWH. Let $\delta\sigma_{\mathrm{PP}}$ be the difference between backscatter coefficients obtained from SASS-II model function [10], [11] using corresponding neutral wind speeds at 19.5 m derived from buoy data with the formulation in [9]. The subscript PP is used to represent HH or VV for horizontal and vertical polarizations, respectively. The backscatter σ_{PP}, measured at the low-wave condition, is adjusted to the wind condition corresponding to the high-wave case as

$$\sigma'_{\mathrm{PP}} = \sigma_{\mathrm{PP}} + \delta\sigma_{\mathrm{PP}}. \tag{1}$$

These adjusted cross section measurements are then used to study the effects of swells on the radar backscatter by comparing with the measured backscatter at the high-wave condition. This normalization method involves incremental differences in the wind speeds and the normalized radar cross section estimates. Thus, the adjusted backscatter coefficient, σ'_{PP}, is not very sensitive to cross-calibrations between SASS and NUSCAT. In addition, if the compared data sets include only in-situ wind measurements from the same buoy, the results will depend only on relative rather than absolute calibrations of the buoy instruments.

B. Large Waves and Moderate Winds

This section investigates the effects of long waves with large SWH on the radar backscatter during moderate wind conditions. In this case, the SASS-II geophysical model function predictions agree with the adjusted results. Fig. 1(a) and (b) show the comparison of NUSCAT radar backscatter measurements near (~10 km) Discus E at 40° incidence angle for vertical and horizontal polarization, respectively. These and the subsequent results are shown as a function of azimuthal angle (relative to upwind; plotted continuously without the 360° wrapping around; this continuous increase in azimuth corresponds to the increase in data acquisition time). In Fig. 1(a), the normalized radar cross section measurements were collected on Mar. 4, 1991 and Mar. 8, 1991. During these measurements, the SWH was 5.5 m on Mar. 4, 1991

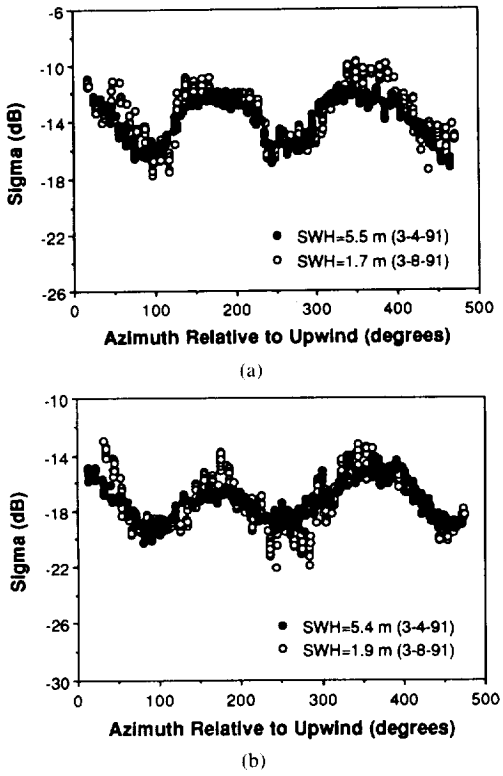

Fig. 1. Comparisons of NUSCAT backscatter coefficients between high-wave cases represented by black circles and low-wave cases denoted with open circles: (a) Vertical polarization corresponding to neutral wind $U_N(19.5) = 12.4\ \mathrm{m \cdot s^{-1}}$ and (b) Horizontal polarization corresponding to neutral wind $U_N(19.5) = 11.8\ \mathrm{m \cdot s^{-1}}$.

and 1.7 m on Mar. 8, 1991. The wind speed was $12.0\ \mathrm{m \cdot s^{-1}}$ on Mar. 4, 1991 and $12.4\ \mathrm{m \cdot s^{-1}}$ on Mar. 8, 1991. All wind speeds discussed in this section are neutral winds at 19.5 m unless otherwise stated. Using (1), this $0.4\ \mathrm{m \cdot s^{-1}}$ wind speed difference reduces σ_{VV} by an average of 0.23 dB. In Fig. 1(b), a case for the horizontal polarization is shown. For this case, the SWH was 5.4 m on Mar. 4, 1991 and 1.9 m on Mar. 8, 1991. The wind was $11.8\ \mathrm{m \cdot s^{-1}}$ on Mar. 4, 1991 and $11.2\ \mathrm{m \cdot s^{-1}}$ on Mar. 8, 1991. The adjustment for the wind speed difference increases σ_{VV} by an average of 0.48 dB. Fig. 1 shows no obvious distinction in the radar backscatter for vertical or horizontal polarization between the low and high SWH data sets.

In addition to these data sets, we also compared low and high SWH data sets at other incidence angles. We have adopted the following approach to present the results in a concise manner. First, wind estimates were obtained from the observed NUSCAT results by fitting the SASS-II model function to the data. These estimates are referred to as the apparent neutral wind speed. Again, the slight differences in actual wind speeds between the low and high SWH data sets need to be accounted for. With the difference δU_N between winds obtained from buoys at high and low-wave conditions, the apparent wind U_N at low SWH is adjusted as

$$U'_N = U_N + \delta U_N. \tag{2}$$

The adjusted winds are then compared with the apparent winds at high SWH to evaluate quantitatively the influence of large waves on radar backscatter during moderate winds.

TABLE I

COMPARISONS BETWEEN HIGH-WAVE (BOLD FACED) AND LOW-WAVE CASES: POL AND θ_0 ARE ANTENNA POLARIZATION AND INCIDENCE ANGLE IN DEGREES, U_N IS THE APPARENT WIND SPEED, U_N^B IS THE BUOY WIND SPEED, AND U'_N IS THE ADJUSTED WIND SPEED. ALL WIND SPEEDS ARE IN $\mathrm{m \cdot s^{-1}}$ AT 19.5 m. THE DIFFERENCE ΔU IS BETWEEN THE ADJUSTED WIND AT LOW SWH AND THE APPARENT WIND AT HIGH SWH AND THE CORRESPONDING PERCENTAGE ERROR IS $\%E$.

DATE	Pol θ_0	U_N U_N^B U'_N	ΔU $\%E$	H_s	T_{air} T_{sea}
91-03-04	**VV 30**	**10.1 10.2 -na-**	**-na- -na-**	**3.56**	**12.1 14.9**
91-03-08	VV 30	10.7 11.2 9.7	−0.4 −4.0	1.58	5.8 8.7
91-02-28	VV 30	11.5 11.8 9.8	−0.3 −3.0	1.47	15.5 20.3
91-02-27	VV 30	11.3 11.5 9.9	−0.2 −2.0	1.70	6.5 19.1
91-03-04	**VV 40**	**11.8 12.0 -na-**	**-na- -na-**	**5.49**	**16.7 20.4**
91-03-08	VV 40	12.6 12.4 12.2	+0.4 +3.4	1.72	7.0 19.5
91-02-28	VV 40	12.0 11.8 12.3	+0.5 +4.2	1.45	15.5 20.3
91-02-27	VV 40	13.0 12.8 12.2	+0.4 +3.4	2.20	7.2 20.6
91-03-04	**HH 20**	**11.9 12.9 -na-**	**-na- -na-**	**5.08**	**15.7 20.4**
91-03-08	HH 20	10.9 11.6 12.3	+0.4 +3.4	1.90	6.7 19.6
91-03-08	HH 20	11.5 11.8 12.6	+0.8 +5.6	1.92	6.3 19.6
91-03-04	**HH 30**	**9.6 10.5 -na-**	**-na- -na-**	**5.27**	**16.0 20.4**
91-03-06	HH 30	11.4 11.4 10.5	+0.9 +9.4	1.83	6.9 19.6
91-02-27	HH 30	11.2 12.8 8.9	−0.7 −7.3	2.20	7.2 20.6
91-03-04	**HH 40**	**10.9 11.2 -na-**	**-na- -na-**	**5.35**	**16.3 20.4**
91-03-08	HH 40	12.0 11.8 11.4	+0.5 +4.6	1.90	6.3 19.6
91-02-27	HH 40	12.3 13.0 10.4	−0.5 −4.6	2.20	7.4 20.6
91-03-04	**HH 60**	**12.3 12.5 -na-**	**-na- -na-**	**5.10**	**15.7 20.4**
91-03-08	HH 60	12.8 11.4 14.0	+1.7 +13.8	1.81	6.9 19.6
91-03-08	HH 60	12.8 11.6 13.7	+1.4 +11.4	1.90	6.6 19.6

Table I gives results of this comparison. The cases are for vertical polarization at incidence angles 30° and 40° and horizontal polarization at incidence angles 20, 30, 40, and 60°. For each case, at least two measurements at low SWH are compared to the corresponding measurement at high SWH. Included in the table are the measurements of SWH, air temperature, and sea temperature. The air temperature was less than the sea temperature in all cases. This indicates the Monin-Obukov stability lengths are negative and thus the atmospheric boundary layer conditions are unstable. The small differences in wind speeds and the percent errors presented in Table I demonstrates no significant effects of swells on the backscatter measurements collected by NUSCAT at Ku-band for moderate wind conditions. Furthermore, the apparent wind speeds derived from the NUSCAT measurements agree well with those obtained from buoys. Fig. 2 compares the apparent wind speed and direction to the buoy measurements of wind speed and direction. The cases shown are for high SWH conditions.

The C-SCAT data were analyzed using similar techniques. The backscatter coefficients σ_{VV} were compared for low and high SWH conditions under moderate winds. Fig. 3 shows a representative example for 40° incidence angle. This data corresponds to the NUSCAT data shown in Fig. 1(a). Both sets were collected during the same flight line. The neutral winds speed for these sets are $12.4\ \mathrm{m \cdot s^{-1}}$ and $12.0\ \mathrm{m \cdot s^{-1}}$ obtained from buoy measurements. The adjustment in backscatter to account for the wind difference is less than 0.3 dB. The comparison in Fig. 3 reveals no visible difference between the magnitude nor the azimuthal modulation of the backscatter measurements.

We compared additional C-SCAT data sets at 20, 30, 40, and 50° incidence angle. At each angle, there were several high and correspondingly low SWH cases. The neutral wind speeds at 10 m ranged from $9.1\ \mathrm{m \cdot s^{-1}}$ to $11.8\ \mathrm{m \cdot s^{-1}}$. Fig. 4(a) and (b) summarize the results. Fig. 4(a) is a plot of the upwind/crosswind ratio versus SWH. There is no observable effect on the upwind/crosswind ratio caused by the large

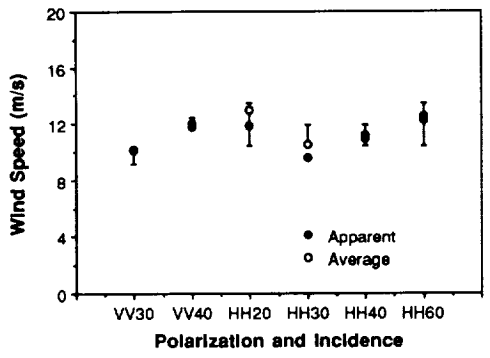

(a)

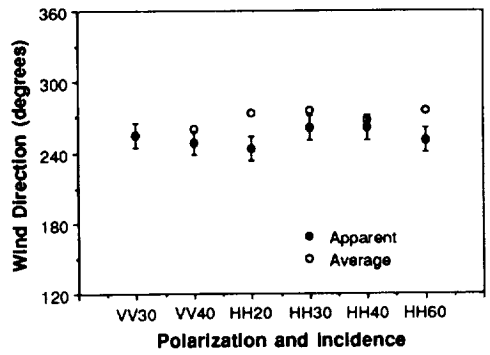

(b)

Fig. 2. Comparisons of wind vectors in the presence of large waves with high SWH on Mar. 4, 1991: (a) Neutral wind speeds at 19.5 m for *apparent* wind from Ku-band data retrieved by SASS-II and *average* wind from buoy data averaged over the duration of the scatterometer data acquisition time T_s, error bars in average winds are determined from buoy data taken before and after T_s; (b) Wind direction for *apparent* wind from Ku-band data and *average* wind from buoy data; error bars in apparent wind directions are due to the NUSCAT 10°-azimuth steps.

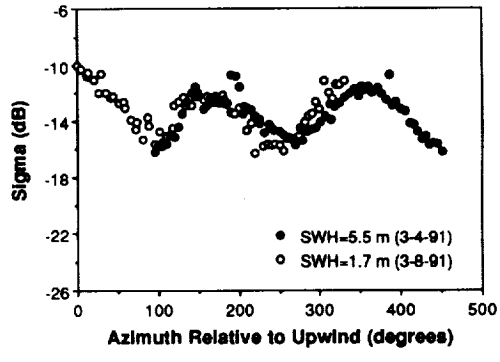

(a)

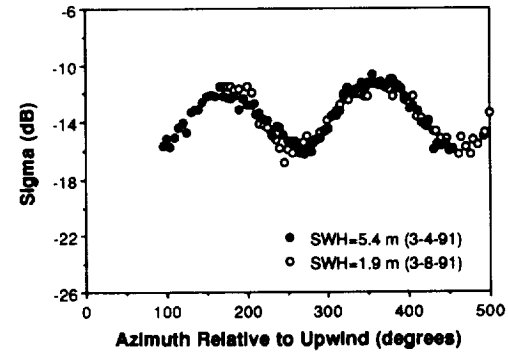

(b)

Fig. 3. Comparison of C-SCAT backscatter coefficients between high-wave case represented by black circles and low-wave case denoted with open circles. The polarization is vertical and the neutral wind speeds are $U_N(19.5) = 12.4\ \mathrm{m \cdot s^{-1}}$ for low wave and $U_N(19.5) = 12.0\ \mathrm{m \cdot s^{-1}}$ for high wave.

waves. Fig. 4(b) displays the average backscatter coefficient versus SWH. The average was performed over the entire 360° for each case. No adjustment is made for the differences in wind speeds. This plot demonstrates no significant change in the magnitude of the average backscatter coefficient at C-band with SWH for moderate winds.

The analysis in this section shows that the differences in backscatter at Ku and C bands with high and low SWH are within the uncertainty of radar (± 1 dB) and wind speed (± 1 $\mathrm{m \cdot s^{-1}}$ or 10% at $U > 10\ \mathrm{m \cdot s^{-1}}$) measurements. Thus, the existence of large waves with high SWH (up to 5.5 m) does not have significant impact on the radar backscatter at moderate wind conditions.

C. Large Waves and Light Winds

During SWADE, a couple of flights occurred during light wind conditions. The SWH varied from 1.7–3.4 m for these data sets. Applying the same criteria defined in Section II-A to these data, we investigated the effects of large waves on the radar backscatter for light winds. The two flights of interest were on Mar. 4, 1991 and Mar. 5, 1991. The data was collected near Discus C. Fig. 14(a) shows the wind and SWH conditions at Discus C during the flight on Mar. 4, 1991. Table VI summarizes the conditions for both flights.

The comparison data, selected after the criteria in Section II-A, were backscatter measurements at horizontal polarization for incidence angles from 20–50° for NUSCAT and at vertical polarization for incidence angles in the same range for C-SCAT. Tables II and III summarize the data for NUSCAT and C-SCAT, respectively. They list the wind speed (measured by buoy at 4-m height), SWH, air temperature T_{air}, and sea temperature T_{sea} obtained from Discus C for each low and high SWH set. The differences in wind speeds between the low and high SWH sets range from 0.1 $\mathrm{m \cdot s^{-1}}$ to 1.3 $\mathrm{m \cdot s^{-1}}$.

Fig. 5(a) and (b) compare data collected at 40° incidence angle for low and high SWH. Fig. 5(a) is a plot of σ_{HH} collected by NUSCAT and Fig. 5(b) is a plot of σ_{VV} collected by C-SCAT. The data is displayed over the full azimuth range and is referenced to the *upwind* direction, defined (for this subsection) as the direction of maximum backscatter. The actual angles will be dealt with later in Fig. 8. The Ku-band measurements are approximately 5 dB higher for the high wave case compared to the low wave. Likewise, the C-band measurements are approximately 4.5 dB higher for the high wave case. Note that the upwind/crosswind backscatter ratio is also affected as seen in these figures; however, a more specific conclusion requires more measured data with various relative azimuth angles including aligned and oblique cases of wind and wave directions. For the above measurements, the air temperature is approximately the same while the sea temperatures are quite different. However, the temperature effects in these cases are insignificant as discussed in appendix A4.

Backscatter for high wave conditions is represented by closed circles in Fig. 6. This data were also collected at 30° incidence angle and horizontal polarization with a sea

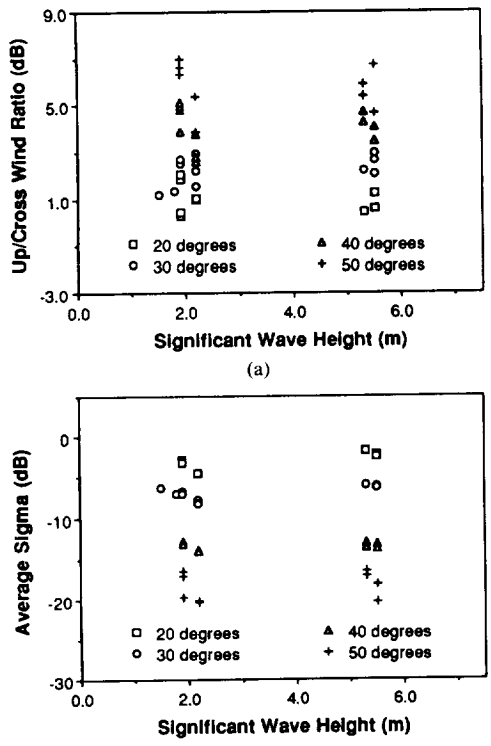

Fig. 4. Comparison of C-SCAT data from 20–50°-degree incidence angles at vertical polarization for high and low-wave cases at 10-m neutral winds from 9.1–11.8 $m \cdot s^{-1}$: (a) Ratio of up/cross wind backscatter coefficients versus significant wave height and (b) Average backscatter coefficients versus significant wave height.

TABLE II
BUOY DATA CORRESPONDING TO HIGH (BOLD FACE) AND LOW-WAVE CASES FOR COMPARISONS OF NUSCAT BACKSCATTER COEFFICIENTS. WIND SPEEDS IS $U(4)$ MEASURED AT 4-m HEIGHT, SIGNIFICANT WAVE HEIGHT IS H_s, AIR TEMPERATURE IS T_{air}, AND SEA SURFACE TEMPERATURE IS T_{sea}.

FLT	DATE	Pol θ_0	$U(4)$ (m/s)	H_s (m)	T_{air} (°C)	T_{sea} (°C)
5	91-03-04	HH 20	3.2	3.0	9.3	14.9
6	91-03-05	HH 20	4.4	1.8	10.2	18.8
5	91-03-04	HH 30	4.9	3.3	11.1	14.9
6	91-03-05	HH 30	4.3	1.7	10.2	18.8
7	91-03-06	HH 30	4.8	1.8	10.8	9.0
5	91-03-04	HH 40	5.5	3.3	11.3	14.9
6	91-03-05	HH 40	4.3	1.7	10.2	18.8
5	91-03-04	HH 50	4.4	3.4	10.6	14.9
7	91-03-06	HH 50	5.1	1.8	10.9	9.0

temperature of 14.9°C. The high SWH measurements show an enhanced radar cross section in comparison to the two low SWH cases. At incidence angles from 20–50°, Fig. 7(a) and (b) compare the conditions corresponding to the cases listed in Table II for NUSCAT and Table III for C-SCAT, respectively. This comparison shows an increase of several dB in the backscatter coefficient between the high and low SWH cases . The difference seems to increase with incidence angle.

Fig. 8(a) and (b) compare the time evolution of the wind vectors deduced from NUSCAT data to the wind vectors obtained from the buoys. The black circles in Fig. 8(a) represent

TABLE III
BUOY DATA CORRESPONDING TO HIGH (BOLD FACE) AND LOW-WAVE CASES FOR COMPARISONS OF C-SCAT BACKSCATTER COEFFICIENTS. WIND SPEED $U(4)$ IS MEASURED AT 4-m HEIGHT, SIGNIFICANT WAVE HEIGHT IS H_s, AIR TEMPERATURE IS T_{air}, AND SEA SURFACE TEMPERATURE IS T_{sea}.

FLT	DATE	Pol θ_0	$U(4)$ (m/s)	H_s (m)	T_{air} (°C)	T_{sea} (°C)
5	91-03-04	VV 20	3.2	2.9	9.3	14.9
10	91-03-10	VV 20	4.5	1.0	5.9	16.0
5	91-03-04	VV 30	5.5	3.3	11.3	14.9
5	91-03-04	VV 40	4.6	3.5	10.4	14.9
10	91-03-10	VV 40	4.5	1.0	5.8	16.0
5	91-03-04	VV 50	5.0	3.3	11.1	14.9
10	91-03-10	VV 50	4.5	1.0	5.8	16.0

the "apparent" wind speed (at 19.5 m) which was obtained by a least-square-error fit of the SASS-II model function to the NUSCAT data collected over Discus C. The open circles are the "average" wind speed derived by translating the buoy wind measurements to 19.5 m using the Large and Pond formulation [9]. The average wind speeds shown at 54, 114, and 174 minutes after 21:00 UT were 8 minute averages recorded by the buoys at 22:00, 23:00, and 24:00 UT. Each average was performed during minutes 50–58 before the recorded hour. The other data points shown were interpolated from these measurements and integrated over the corresponding duration of the NUSCAT measurement. Fig. 8(b) shows the principal directions of the peak wave components obtained from the NDBC directional wave spectrum measurements. The wave direction is defined as the angle from North to the direction to which the wave propagates. The wave data from the buoy are measured from minute 28–48 each hour. The average is plotted at minute 38 before the hour. The other wave data points correspond to time-interpolated buoy data over the scatterometer time.

As Figs. 8(a) and 14(a) show, the wind speed at Discus C dropped quickly at the beginning of the flight to a light wind speed, and then began to increase during the flight. Coastal Buoy 2 shows similar conditions. The apparent winds in Fig. 8(a) are higher than the average winds, implying that the observed backscatter is higher than the model function estimates for the given buoy wind. Both the apparent wind and the average wind follow the same trend. They drop in the beginning of the flight and then increase slightly towards the end. In the latter part of the flight, the apparent wind becomes closer to the average wind. The direction of the apparent wind, shown in Fig. 8(b), appears to be different from both the average wind direction and the principle wave direction. Towards the end of the flight, the apparent wind direction appears to be closer to the average wind direction. For the times shown, the peak wave direction was between 340–360° and the SWH was between 3 and 4 m.

For light winds, the data presented in this section indicate that ocean radar backscatter is larger in cases of high waves especially at larger incidence angles. These observations were seen in both Ku-band and C-band backscatter while similar ocean conditions (see Fig. 14) were measured by two nearby (~30 km) buoys Discus C and Coastal Buoy 2 (see buoy locations in Fig. 13).

III. COMPARISONS WITH MODELS

The experimental measurements obtained by NUSCAT and C-SCAT are compared with calculated results from empirical

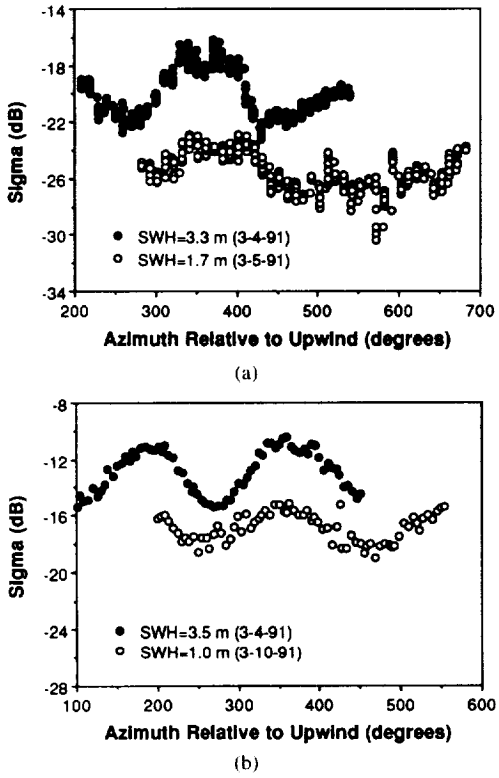

Fig. 5. Comparisons of backscatter coefficients at 40° incidence angle at wind speeds $U(4) \sim 4$-5 $\mathrm{m \cdot s^{-1}}$ measured by buoys at 4-m height between high-wave cases represented by black circles and low-wave cases denoted with open circles: (a) NUSCAT horizontal polarization and (b) C-SCAT vertical polarization.

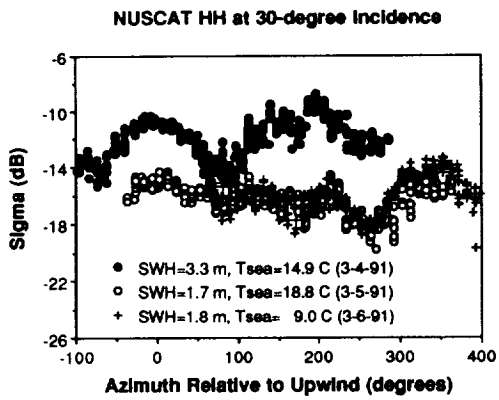

Fig. 6. Comparisons of NUSCAT backscatter coefficients (buoy wind $U(4) \sim 4$-5 $\mathrm{m \cdot s^{-1}}$) at horizontal polarization and 30° incidence angle between high-wave case represented by black circles and low-wave cases denoted with open circles and plus signs at different sea surface temperatures.

models such as SASS-II [10], [11] for Ku band, CMOD3-H1 for C band [12], and Plant's theoretical model [5], [6] for both frequencies. Fig. 9(a) shows the comparisons between the models and NUSCAT data at vertical polarization and 40° incidence angle. NUSCAT data plotted with open squares in Fig. 9(a) are the same as those for the large wave case in Fig. 1(a) (SWH = 5.5 m on Mar. 4, 1991). SASS-II results represented by the thick curve are calculated from the model function. The wind was calculated to be 12.0 $\mathrm{m \cdot s^{-1}}$ at a height of 19.5 m using the buoy data. The thin curve is the calculated results from Plant's model for wind-generated waves using a 10-m wind of 11.3 $\mathrm{m \cdot s^{-1}}$ derived from the 19.5 m wind used

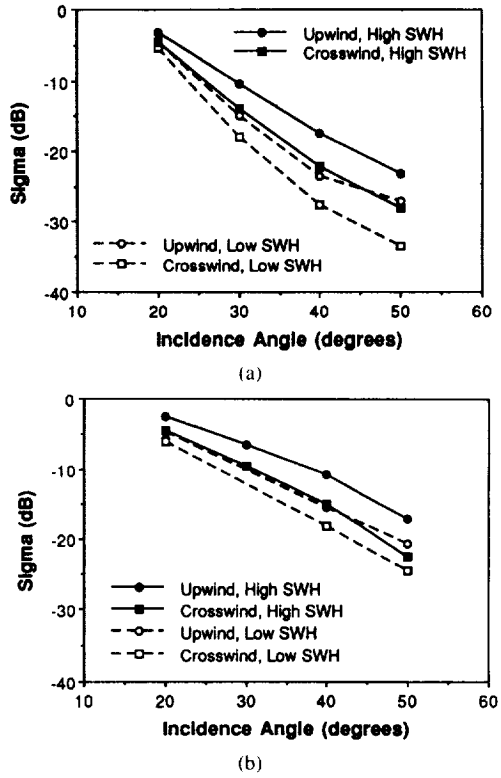

Fig. 7. Comparisons of backscatter coefficients versus incidence angles in the upwind and crosswind directions between high-wave cases represented by black symbols and low-wave cases denoted with open symbols: (a) NUSCAT horizontal polarization and (b) C-SCAT vertical polarization.

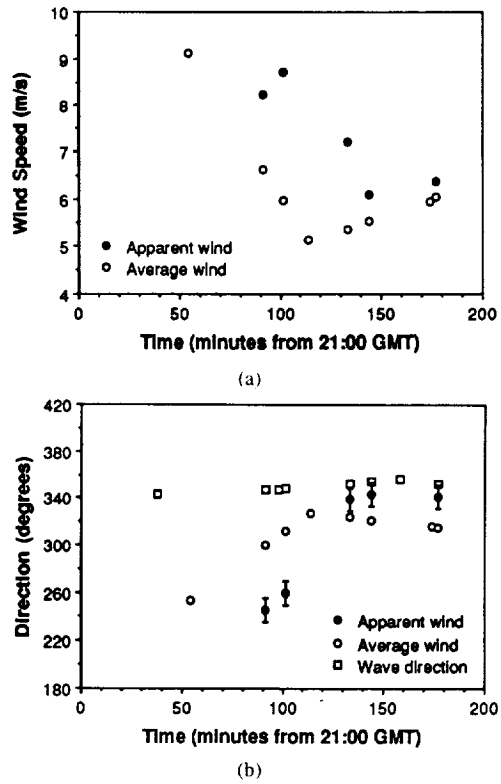

Fig. 8. Time evolution of (a) Wind speeds and (b) Wind directions. Directions of dominant waves are also shown.

in SASS-II. While the models do not include swells, all results match well. This again indicates that the effect of the large waves at moderate winds is not significant in our case study.

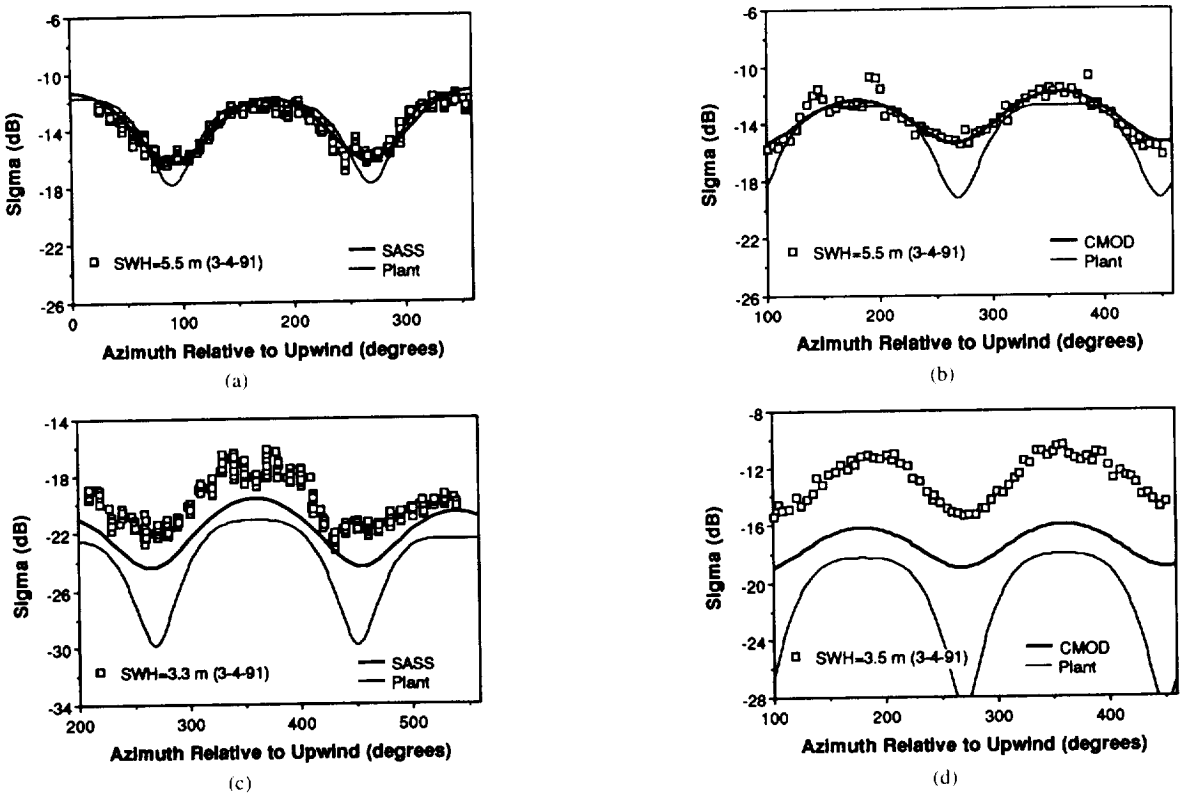

Fig. 9. Comparisons of measured backscatter coefficients (squares) in the presence of swells at 40° incidence angle to results calculated from empirical models (thick curves) and Plant's theoretical model (thin curves). For moderate wind (a) NUSCAT vertical polarization for $U_N(10) = 11.3\ \mathrm{m \cdot s^{-1}}$ and (b) C-SCAT vertical polarization for $U_N(10) = 11.3\ \mathrm{m \cdot s^{-1}}$. For light wind (c) NUSCAT horizontal polarization for $U_N(10) = 6.6\ \mathrm{m \cdot s^{-1}}$ and (d) C-SCAT vertical polarization for $U_N(10) = 5.4\ \mathrm{m \cdot s^{-1}}$.

Similarly, the models are compared with the C-band data corresponding to the above Ku-band data. The results are shown in Fig. 9(b). Both the CMOD3-H1 and Plant's model use the wind $U(10) = 11.3\ \mathrm{m \cdot s^{-1}}$ derived from the buoy data. The models agree well with the data except at the crosswind direction where Plant's model underestimates the backscatter. Theoretical results at C band are obtained from Plant's model using input parameters determined with Ku-band backscatter data.

In the case of high SWH and light winds, the data presented in panels (c) and (d) of Fig. 9 correspond to the high SWH cases shown in Fig. 5. The incidence angle in this figure is 40°. In the model calculations, $U(19.5) = 6.6\ \mathrm{m \cdot s^{-1}}$ and $U(10) = 6.3\ \mathrm{m \cdot s^{-1}}$ are used in the SASS-II and Plant's models for Ku band, respectively. Results at C band are calculated from the CMOD3-H1 and Plant's models using $U(10) = 5.4\ \mathrm{m \cdot s^{-1}}$. The Ku-band measurements are as much as 4 dB higher than SASS-II results and C-band data are more than 4 dB larger compared to CMOD3-H1 values; the high backscatter data apparently correspond to wind speed in the range of 10-12 $\mathrm{m \cdot s^{-1}}$ deduced from the model functions. Plant's model for both frequencies gives even larger backscatter differences compared to the other two models.

A mechanism for large wave effects on backscatter is the superposition of a large-scale roughness caused by swells on the wind-generated roughness. Reference [3] estimated that a large magnitude swell of 16 m in SWH or 4 m in root-mean-square height with a 300-m wavelength could cause 4.5–3 dB increase in Ku-band horizontal backscatter at 20° and only 1.5–1 dB at 50° for wind speeds at 5–10$\mathrm{m \cdot s^{-1}}$. In the same wind speed range, an increase of 6-4.5 dB at 20° and 3–1.5 dB at 50° incidence angle was obtained for L-band backscatter. This model predicts that the effects of swells decrease as the incidence angle increases because at small incidence angles, the backscatter is partly due to specular return; while at large incidence angles, specular return is negligible. This wave superposition mechanism predicts a trend with incidence angle different from that observed in the data.

Another potential mechanism that contributes to the backscatter is wave breaking. Reference [13] showed that long waves moving across the surface can augment the surface drift near the long-wave crests; consequently, the maximum amplitude of the short waves before breaking is reduced and the number of waves breaking is increased. In the results shown in [14], the backscatter due to wave breaking was suggested to be directly related to the cubic magnitude of the friction velocity and therefore increases as the friction velocity increases. The backscatter measurements in this paper, however, show the opposite trend.

Ocean radar backscatter has been suggested to be closely related to the friction velocity, u_* [15]. Let's consider the variations in u_* in the presence of swells measured during SWADE. The Small Water Plane Area—Twin Hull, SWATH, ship Frederick G. Creed was chartered and equipped to perform measurements, including u_*, in support of SWADE [16]. For the above large-wave cases, the flight lines did not pass

TABLE IV

RESULTS FOR u_*, MEASURED BY THE SWATH SHIP, UNDER LIGHT WINDS IN THE PRESENCE OF LARGE WAVES. T_{air} IS AIR TEMPERATURE, T_{sea} IS SEA SURFACE TEMPERATURE, H_s IS SIGNIFICANT WAVE HEIGHT, ϕ_{wave} IS FOR DIRECTION TO WHICH WAVES PROPAGATE, $U(12.9)$ IS WIND SPEED MEASURED AT 12.9-m HEIGHT, ϕ_{wind} IS WIND DIRECTION, EXP. u_* IS FROM THE EXPERIMENT IN THE PRESNECE OF SWELLS, AND CAL. u_* IS CALCULATED [14] WITHOUT SWELL.

SWATH	DATE	TIME (UT)	LATITUDE(N) LONGITUDE(W)	T_{air} (°C) T_{sea} (°C)	H_s (m) ϕ_{wave} (°)	$U(12.9)$ (m · s^{-1}) ϕ_{wind} (°)	Exp. u_* (m · s^{-1}) Cal. u_* (m · s^{-1})
24	91-03-05	21:09	36°50′ 74°00′	11.0 18.8	2.5 324	3.3 310	0.16 0.13
25	91-03-05	23:09	37°00′ 74°10′	11.5 19.5	1.9 315	3.7 284	0.26 0.14
27	91-03-06	17:17	37°17′ 73°27′	16.0 19.6	2.1 315	6.9 175	0.37 0.25
29	91-03-07	20:32	43°00′ 74°26′	11.2 12.5	2.2 311	4.9 310	0.27 0.17

TABLE V

RESULTS FOR u_*, MEASURED BY THE SWATH SHIP, UNDER MODERATE WINDS IN THE PRESENCE OF LARGE WAVES. T_{air} IS AIR TEMPERATURE, T_{sea} IS SEA SURFACE TEMPERATURE, H_s IS SIGNIFICANT WAVE HEIGHT, ϕ_{wave} IS FOR DIRECTION TO WHICH WAVE PROPAGATES, $U(12.9)$ IS WIND SPEED MEASURED AT 12.9-m HEIGHT, ϕ_{wind} IS WIND DIRECTION, EXP. u_* IS FROM THE EXPERIMENT IN THE PRESENCE OF SWELLS, AND CAL. u_* IS CALCULATED [14] WITHOUT SWELL.

SWATH	DATE	TIME (UT)	LATITUDE(N) LONGITUDE(W)	T_{air} (°C) T_{sea} (°C)	H_s (m) ϕ_{wave} (°)	$U(12.9)$ (m · s^{-1}) ϕ_{wind} (°)	Exp. u_* (m · s^{-1}) Cal. u_* (m · s^{-1})
16	91-03-04	18:56	36°09′ 75°15′	13.5 11.0	2.9 330	9.7 200	0.33 0.30
18	91-03-05	01:00	35°49′ 75°04′	12.1 14.5	2.7 330	9.7 253	0.40 0.33
19	91-03-05	02:00	35°49′ 75°09′	11.9 14.0	2.6 342	8.6 277	0.37 0.30
20	91-03-05	03:08	35°49′ 75°09′	11.8 14.0	2.2 324	8.8 288	0.41 0.30

over the temporal or spatial vicinity of the SWATH ship; therefore, co-located measurements of u_* were not available to correlate with the scatterometer observations. Instead, u_* measurements in the presence of large swells are evaluated for a qualitative comparison. Tables IV and V show the times, locations, atmospheric and oceanic parameters for these cases.

In these swell cases, data from the SWATH ship show measured values of u_* corresponding to the larger values found in the last column of Table IV. For instance, in SWATH ship Run 25 started at 23:09 on Mar. 5, 1991, the friction velocity was 0.26 m · s^{-1} and the neutral wind speed was 3.72 m · s^{-1}. At this neutral wind speed and the measured air and sea temperatures, Large and Pond's formula [9] gives $u_* = 0.14$ m · s^{-1} without consideration of swell effects. The difference between the value of u_* without swell and the measured value with swell is 0.12 m · s^{-1}. With the exception of Run 24, all other cases in Table V show differences in the order of 0.1 m · s^{-1} between u_* measurements in the presence of swells compared to u_* calculations without swell. Similar increments in u_* are observed in moderate wind conditions (8.6–9.7 m · s^{-1} at 12.9 m) in the presence of large wave of equivalent SWH. These results are summarized in Table V.

The above observations lead to the hypothesis that the increase of u_* in the presence of swells is responsible for the effects in the observed backscatter. Fig. 10 presents the backscatter calculated with a model function relating the mean normalized radar cross section to u_* [17]. This model was developed based on the backscatter measured by the JPL Ku-band Airborne Microwave Scatterometer and the measured u_* during the Frontal Air-Sea Interaction Experiment. The results in Fig. 10 show that an increase of 0.1 m · s^{-1} in u_* (as suggested by the SWATH ship measurements in the swell cases) can give rise to a 3.5-dB increase in σ_{HH} at 30° and a 4.5-dB increase at 50° incidence angle at light wind conditions. For the same magnitude of increment in u_* at moderate winds, the change in the backscatter is less significant (σ_{HH} varies only by 1.5 dB) compared to the case of light winds as seen in Fig. 10. These results follow the observations of the backscatter in the presence of swells.

Another trend in the observed backscatter for the swell cases is that the increase in the backscatter is less at small incidence angles (see Fig. 7). At the small angles, ocean backscatter coefficients measured by scatterometers [8] ,[18]–[20] become less sensitive to wind variations. Moreover, in the power-law model function relating mean backscatter to u_* [17], the exponent of u_* for 30° incidence angle is about 20% less than that for 50°. Hence, the increase in u_* will result in a weaker increase in the backscatter at small angles of incidence. This corresponds to the small enhancement at small incidence angles observed in σ_{VV} and σ_{HH}, shown in Fig. 7 for the Ku- and C-band frequencies. Thus, the increase of the friction velocity in the swell cases also gives the same trend of smaller increase in backscatter at small incident angles as seen in the measurements.

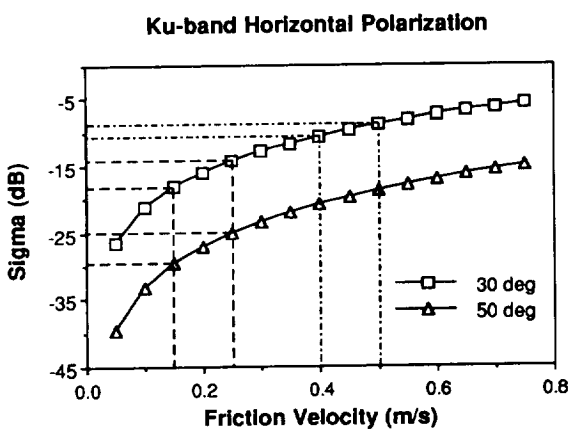

Fig. 10. Backscatter coefficient σ_{HH} at Ku band versus friction velocity at 30° and 50° incidence angle. The results are obtained from the model function relating mean backscatter to friction velocity [17].

In summary, the backscatter measurements at Ku and C bands obtained during SWADE were used to study the behavior of the backscatter in the presence of large waves. The experimental observations are: 1) For moderate wind conditions, there was no obvious difference between the backscatter measurements observed for low and high SWH; 2) For light winds, however, the backscatter coefficients were significantly enhanced in the presence of large swells; and 3) The enhancement also seemed to increase with incidence angle, especially for the Ku-band data. These observations are different from the trends predicted by wave superposition [3] and wave breaking [13], [14] mechanisms. However, an increase of the friction velocity in the presence of swells can lead to results which agree with the experimental observations.

IV. Appendix

A1. NUSCAT and C-SCAT Scatterometers

During SWADE, NUSCAT and C-SCAT, the two airborne scatterometers, collected backscatter data. NUSCAT is a Ku-band system operating near 14 GHz. The system comprises of an antenna subsystem, an RF subsystem, a data collection subsystem, and a controller as illustrated in Fig. 11(a). The antenna is a parabolic dish with a peak gain of 32 dB and a 2-way equivalent beamwidth of 4°. The antenna was placed inside a radome on the tail of the C-130B aircraft (Fig. 12), and was mounted on a gimbal, which was used to rotate it in complete azimuthal scans at selected elevation (incidence) angles. The antenna subsystem is connected through a rotary joint to the RF subsystem, from which horizontally (H) or vertically (V) polarized pulses are transmitted with a peak power of either 10 or 250 W at a repetition frequency of 4 to 10 kHz and a pulse length of 15–75 μs. When the system transmits either H or V polarization, two receivers collect simultaneous co- and cross-polarized returns. The radar echoes from each pulse are amplified, down-converted to I/Q samples and digitally square-law detected. The returns from multiple echoes are integrated over a 0.5 second interval, and then recorded on computer compatible tapes.

C-SCAT is a pulsed, low-power scatterometer operating with vertical polarization in the frequency band of 4.98–5.70

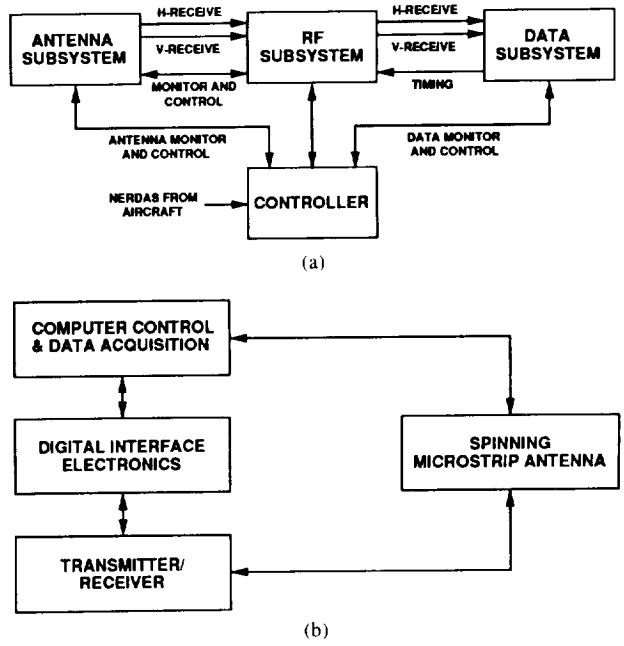

Fig. 11. Scatterometer system block diagrams: (a) NUSCAT and (b) C-SCAT.

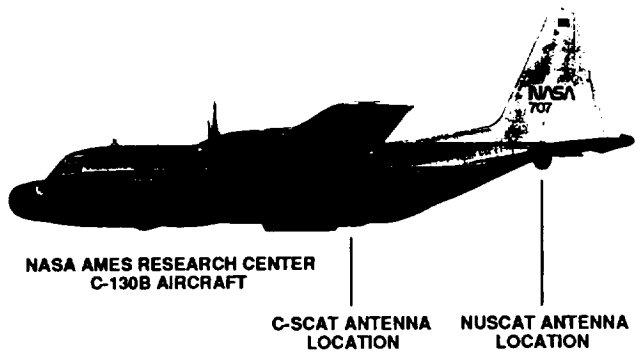

Fig. 12. Locations of NUSCAT and C-SCAT antennas on the NASA Ames Research Center C-130B aircraft.

GHz with a peak power of 2 W. The radar system consists of a spinning antenna, a transmitter/receiver subsystem, digital interface electronics, and a computer control and data acquisition subsystem shown in Fig. 11(b). The antenna is a flat microstrip array with a peak gain of 28 dB and a 2-way equivalent beamwidth of about 5°. A spinning mechanism rotates the whole antenna in a full azimuthal circle at around 20 rpm. The incidence angle can be steered from 20 to 50° by frequency scanning. The transmitted pulse duration is adjusted with aircraft altitude as an input to maximize the signal-to-noise ratios of the received echoes. Further details of C-SCAT have been reported in [21].

The internal system calibration for NUSCAT is performed by injecting the transmit signal into the receiver through a calibration loop. The relative calibration accuracy involves the uncertainty in the measurements of transmitted power, receiver gain, the orientation angles of the antenna, the aircraft altitude, the rotary joint loss, the radome loss and the attenuators. The relative calibration accuracy is estimated to be ± 0.23 dB. The measured radar backscatter accuracy depends on the number of independent samples and the signal-to-noise ratio (SNR). The

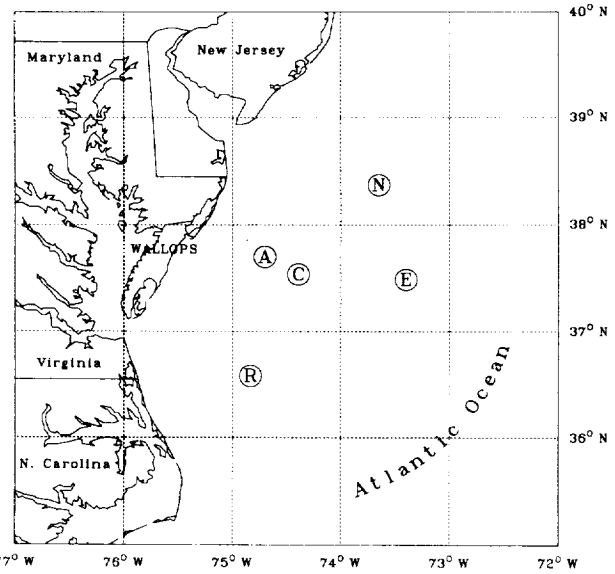

Fig. 13. Geographical location where the Surface Wave Dynamics Experiment was carried out. Encircled capital letters denote buoy positions: A is the NOAA Coastal Buoy 2, C is Discus C, E is Discus E, N is Discus N, and R is CERC.

operating frequency was dithered over 100 MHz to generate additional independent samples (N) which effectively reduce the statistical fluctuation of the detected power by $1/\sqrt{N}$. For the observations reported in this paper, N is between 750 and 5000. It should be noted that the SNR and the accuracy of the noise-only measurements was high enough that the backscatter power accuracy was primarily determined by the number of independent samples. The absolute accuracy of NUSCAT was subjected to other error sources such as attenuator loss, calibration loop loss, antenna gain, beamwidth, and various losses from the waveguide and the rotary joint. The antenna gain was determined by the three-horn measurement method at the JPL antenna range. The system stability and absolute accuracy were evaluated by taking data over the ocean surface at 10° incidence angle, where the backscatter is insensitive to surface roughness conditions [19]. These in-flight calibrations were performed at the beginning and the end of each flight line during SWADE. Based on these measurements, our estimated absolute error is about ± 1 dB.

C-SCAT is subject to the same sources of error as NUSCAT, and requires similar calibration measurements. The internal system is calibrated by feeding part of the transmit signal into the receiver through a series of attenuators to calibrate out system fluctuations, which are typically less than 0.1 dB during a flight. Additionally, the C-SCAT system was absolutely calibrated using a trihedral corner reflector at the UMass campus and a sphere at Goldstone, CA. The relative precision is better than 0.25 dB, and the absolute accuracy is estimated to be within 1 dB [21].

During SWADE, the NUSCAT antenna was stepped in azimuth for 10° once every 4 seconds. NUSCAT collected azimuthal scans of data at various incidence angles, ranging from 0–60° in 10° increments. The C-SCAT antenna was rotated at 20 rpm, and the backscatter data were averaged into 5° azimuthal bins. Each rotation collects approximately 30 independent samples in each bin, and the data from at least 2 azimuthal scans were averaged together to obtain a stable average of the normalized radar cross section. C-SCAT collected azimuthal scans of data at incidence angles ranging from 20–50° in 10° increments.

In both the NUSCAT and C-SCAT data, the aircraft speed, altitude, latitude, longitude, yaw, pitch and roll angles were recorded. The actual values of the incidence and azimuthal angles were calculated from the commanded pointing angles and the aircraft pitch and roll angles. The variations in the aircraft pitch and roll induced fluctuations in the incidence angles at which the radar data was taken. For the NUSCAT data, the SASS-II model function [10], [11] was chosen to adjust the backscatter values due to the fluctuations in incidence angle. These variations were subtracted from the measured data to obtain values corresponding to the commanded incidence angle. This technique has been shown to be relatively insensitive to the model function chosen for the range of wind speed and incidence angle variations [22]. A similar procedure was applied to the C-SCAT data base, with the fitting harmonic function derived from the C-SCAT data base.

A2. SWADE Experimental Scenario

The Surface Wave Dynamics Experiment (SWADE) occurred in Oct. 1990 to Mar. 1991. Among its purposes was to study the effects of large waves on ocean backscatter. The experimental area, located off the coast of Maryland and Virginia (as depicted in the map in Fig. 13), was an instrumented ocean area. As the map shows, several buoys are anchored in the area: Discus C (C), Discus E (E), Discus N (N), CERC (R), and the National Oceanographic and Atmospheric Administration's Experimental buoy, or Coastal Buoy 2 (A). During the experiment, NUSCAT and C-SCAT were flown on the C-130B aircraft to take radar backscatter data over ocean surfaces. There were a total of 10 flights during the period Feb. 2, 1991 to Mar. 9, 1991. The flights were partitioned into flight lines, and each line into runs. Flight patterns among the buoys included straight, triangle and radiator patterns. The oceanic conditions encompassed wind speeds ranging from 2–12 $\mathrm{m \cdot s^{-1}}$ and significant wave heights ranging from below 1 m to above 5 m. Table VI summarizes the flight patterns for the 10 flights, together with the atmospheric and oceanic parameters measured by the buoys.

During flight 5 on Mar. 4, 1991, backscatter data were acquired between 20:10 and 00:15 (UT) the following day. Although the wind was from the West, the wave field was dominated by a large swell from the South. The buoy measurements from the National Data Buoy Center (NDBC) provide a synoptic view of the sea conditions. In Fig. 14, the wind speed at 4 m above the ocean surface (top panel), wind direction (middle panel), and significant wave height (bottom panel) obtained by 3 buoys are plotted as functions of time, with the flight time indicated by bold horizontal bars over the time scale. The wind data were averaged for a duration of 8 minutes from 10 to 2 minutes before the tag hour; e.g., the wind data obtained between 22:50 and 22:58 were averaged and reported as the average wind speed at 23:00. The wave data is averaged from 28–48 minutes before the hour, and similarly recorded.

TABLE VI

FLIGHT PATTERNS AND OCEAN CONDITIONS DURING SWADE. THE UNIT FOR FLIGHT TIME IS UT, WIND VECTOR $\vec{U}$ IS $m \cdot s^{-1}$ FOR SPEED AND DEGREE FOR DIRECTION (MEASURED AT 4-m HEIGHT), AND SIGNIFICANT WAVE HEIGHTS H_S IS m. EVENTS REPRESENTED BY BOLD-FACED CHARACTERS ARE USED FOR THE COMPARISON OF HIGH AND LOW WAVES AT MODERATE WIND SPEEDS; EVENTS REPRESENTED BY ITALIC CHARACTERS ARE FOR THE COMPARISON AT LIGHT WINDS

FLT	DATE	TIME (UT)	FLIGHT PATTERN	$\vec{U}(4)$ ($m \cdot s^{-1}$,°) CERC	C	E	H_s (m) CERC	C	E
1	91-02-27	18:30-00:10	Between A, C, and E	1.7-9.1 302-274	6.3-9.9 277-277	9.8-11.6 294-312	1.1-1.6	1.4-1.9	2.0-2.8
2	91-02-28	21:00-00:40	Triangle A, C, CERC then between A and C	3.4-6.1 225-194	8.4-12.6 215-218	9.6-12.1 229-228	0.9-1.0	1.1-1.6	1.3-1.8
3	91-03-01	22:00-01:50	Between A, C, and E	3.2-8.4 142-169	6.3-8.1 182-172	5.4-9.7 192-188	0.9-1.3	1.0-1.1	0.9-1.2
4	91-03-02	21:00-00:50	Between A, C, and E Some rain at altitude	6.0-11.7 233-195	6.2-8.8 271-194	8.8-13.0 270-209	2.9-3.2	3.0-3.3	3.6-4.1
5	91-03-04	20:00-00:30	Triangle C, N, and E Between A, C, and E	6.8-8.9 235-239	*4.2-9.2* *327-251*	**8.8-12.0** **277-259**	2.9-3.4	*3.3-3.7*	**4.3-5.6**
6	91-03-05	18:30-00:10	Past N, in star pattern Between CERC-E, C-E	*2.5-7.1* *322-313*	4.5-6.0 281-279	3.7-7.8 329-325	*1.7-2.0*	1.9-2.2	2.5-2.9
7	91-03-06	22:30-02:00	Triangle C, N, and E then between C and E	7.4-8.8 192-176	10.8-13.1 196-198	9.5-11.4 221-214	1.6-1.6	2.1-2.5	2.2-2.6
8	91-03-07	20:30-02:20	5-leg radiator A, C, E, N then between C and E	2.5-6.8 318-341	6.0-10.3 318-327	10.1-12.3 333-328	1.4-1.9	2.2-2.5	2.0-2.5
9	91-03-08	20:30-00:30	Triangle C, N, and E then between C and E	8.3-10.0 329-336	7.6-9.3 322-328	**9.9-11.0** **348-343**	1.4-1.7	1.4-1.6	1.7-1.9
10	91-03-09	20:30-02:40	Between A, C, and E	5.3-6.2 348-343	4.6-7.0 321-327	6.4-7.6 339-347	1.5-1.7	1.2-1.7	1.3-1.6

The plots in Fig. 14(a) at Discus E on Mar. 4, 1991 reveal a very strong wind, up to 16.7 $m \cdot s^{-1}$, from 237°. This strong wind occurred approximately three hours before the flight and dropped to a moderate westerly wind of 10 $m \cdot s^{-1}$ during the flight. Similarly, the wind speed at Discus C subsided from moderate to a light wind, as low as 4.2 $m \cdot s^{-1}$, and then picked up again at the end of the flight (see the black circle curve in Fig. 14(a)). The wind direction observations at Discus N, Discus E, and at CERC from 21:00 on Mar. 4 through 00:00 on Mar. 5 ranged from 235–277°. At Discus C, only the last two observations were outside this range (327° and 116°). The dominant long-wave wavelength at Discus E was 244 m throughout this four hour flight, and its direction of propagation was within 5° of 357°. At Discus N, the dominant wavelength fluctuated between 244 m and 192 m, and the direction of propagation was within 5° of 349°. The SWH varied spatially, being the highest (5.6 m) at the discus buoy furthest offshore (E), and the lowest (3.4 m) at the discus buoy furthest to the West (CERC) at 21:00. The wave height slowly decreased over the experiment during the four hour period (at 00:00, Mar. 5, 1991, the SWH was 5.1 m at Discus E and 2.9 m at CERC).

The range of wind speeds corresponding to the swell cases is similar to the wind range encountered in several other flights where the wave heights were lower (see Table VI). For example, the SWH at buoy E on Mar. 8 in flight 9 was 2.5 m or less while the wind speed at 4 m above the ocean surface was in the moderate range of 10-12 $m \cdot s^{-1}$, which overlaps the wind speed range in the case with the large SWH (Discus E, Mar. 4, flight 5). For light winds, Table VI indicates that the wind speeds cover an overlapping range at Discus C during flight 5, and during flight 6 at CERC, while the SWH measured at the buoys are different by a factor of 2. This data set presents an opportunity to study the effect of large waves on ocean backscatter by comparing backscatter coefficients at Ku and C bands for cases with low and high waves under similar wind conditions. Furthermore, data from the Scanning Radar Altimeter are available for the swell characterization with directional wave fields shown in the next section.

A3. Directional Wave Fields

Fig. 15 shows four directional wave spectra obtained by the Scanning Radar Altimeter (SRA) on westerly ground tracks. The spectrum in the top panel (A) was acquired at 21:04:26 from 625 m altitude near Discus E and the results are compared with the 21:00 Discus E observations. The along track and cross track spacings of the SRA data to generate the directional wave spectra were 12.2 and 7.8 m, respectively, making it impossible to observe wavelengths shorter than about 25 m propagating in an easterly direction and about 16 m propagating in a northerly direction. The direction of propagation is in good agreement with the buoy observations. Both the SRA directional wave spectrum and the Discus E nondirectional wave spectrum indicate a wave system concentrated in the longer wavelengths.

The SRA spectrum in the second panel (B) of Fig. 15 was acquired at the same position as the one in panel A, but two hours later, and it is compared with the Discus E data at 23:00. This SRA spectrum and the two below it were generated from data acquired from an altitude of 1250 m, with the footprint

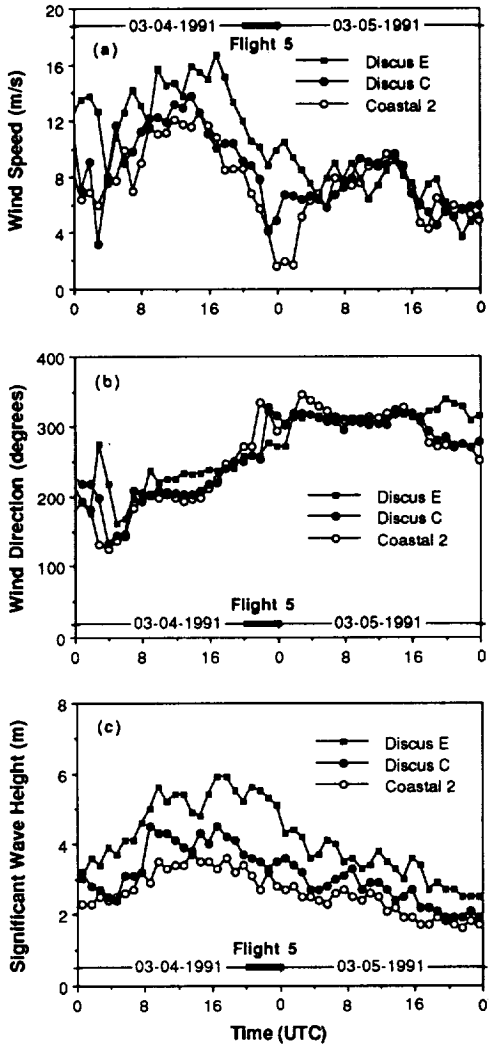

Fig. 14. Data for (a) Wind speeds at height of 4 m and (b) Significant wave heights measured by Discus E and Discus C about one day (Mar. 4, 1991) before Flight 5 for scatterometer measurements until one day (Mar. 5, 1991) after the flight. The flight duration is indicated with the bold horizontal bar.

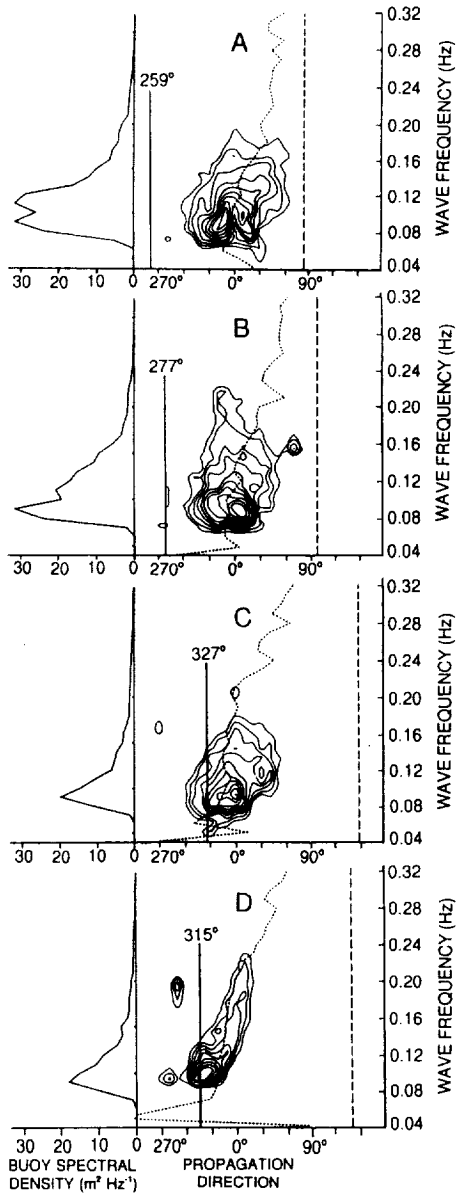

Fig. 15. Directional wave spectra measured by the NASA Scanning Radar Altimeter compared with the direction of propagation and spectral variance density measured by SWADE pitch-and-roll buoys. The contour lines on the right side of the figure indicate SRA measurements of absolute spectral density in 1.5 dB increments above a floor of 0.02 m^2 Hz^{-1} per degree. The dashed curves on the right side indicate the direction of propagation measured by the buoy. The continuous vertical lines indicate the direction from which the wind was blowing and the dashed vertical lines represent the direction toward which the wind was blowing (to be consistent with the wave propagation directions). The top panel (A) compares a SRA wave spectrum measured at 21:04:26 in the vicinity of N 37.5°, W 73.5° with the Discus E 21:00 observations. The second panel (B) compares a 22:58:13 SRA spectrum at the same location with the 23:00 Discus E observations. The third panel (C) compares a 23:02:39 SRA spectrum acquired near N 37.51°, W 73.85° with the 23:00 Discus C observations, and the bottom panel (D) compares a 23:17:25 SRA spectrum near N 37.73°, W 74.84° with the 00:00 Discus C observations on Mar. 5, 1991.

and cross track elevation point spacing double what they were for the top panel. Despite the change in measurement geometry and the passage of time, the two spectra are essentially the same. The third panel (C) was acquired at 23:02:39 midway between Discus E and Discus C. We used it to compared to the Discus C observations at 23:00.

The wave field is significantly reduced at the Discus C position relative to Discus E, but the same trend in propagation direction with increasing frequency is persistent. The spectrum in the bottom panel (D) was acquired at 23:17:25, just inshore of the Coastal Buoy 2. It is compared with the 00:00 Discus C observations from Mar. 5, 1991. Panels C and D indicate that the wave field at Discus C changed little temporally over that hour interval, but the direction of propagation at the spectral peak measured by SRA changed spatially, shifting about 40° toward the West as the SRA moved closer to shore. This is probably an influence of the shallower water close to shore. Panels A and B of Fig. 15 indicate that the wind direction in the vicinity of Discus E was approximately at right angles to the direction of propagation at the peak of the directional wave spectrum at Discus E. Panel D indicates that the wind was nearly opposite to the dominant wave direction near Coastal Buoy 2. Fig. 14 indicates that the wind at Coastal Buoy 2 and Discus C abruptly shifted about 70° northward at 22:00 and 23:00, respectively. This was the same interval when the wind

speed was decreasing rapidly, and these recent light winds had not had time to influence even the higher frequencies (0.32 Hz) of the buoy spectra shown by the dashed lines in panels C and D of Fig. 5(a). These directional wave spectra together with the buoy data provide the basis for the study on backscatter in the presence of swells.

A4. Sea Surface Temperature

In the comparison of backscatter for the cases of large wave and light wind conditions (Section II-C), there are differences in the sea surface temperature. Hence, the effects of the sea temperature need to be investigated to isolate the effects of the swells.

The difference in sea surface temperature can cause a difference in the viscosity. In turn, the viscosity can affect the roughness of the sea surface for a given wind speed. Donelan and Pierson [4] indicate that the backscatter increases as the temperature of the sea increases and that this effect can be significant at light winds when the temperature difference is large (0–30°C). For the temperature range 14–36°C, wave tank measurements [23] at X band (vertical polarization) showed no observable difference in the backscatter at winds $U(19.5)$ from 5–25 $\mathrm{m \cdot s^{-1}}$.

To evaluate the effects of sea temperature on our data, two cases will be considered where all parameters are essentially the same except for the sea temperature. If sea surface temperature plays a dominant role, the backscatter should be higher in the case where the temperature is higher. On Mar. 5, 1991 and Mar. 6, 1991 the sea temperature was 18.8°C and 9.0°C, respectively. Table II gives a summary of the conditions and Fig. 6 compares the data, showing backscatter measurements at 30° incidence angle, horizontal polarization during low wave conditions. Open circles represent the data collected for $T_{\mathrm{sea}} = 18.8$°C on Mar. 5, 1991 and pluses represent data collected for $T_{\mathrm{sea}} = 9.0$°C on Mar. 6, 1991. The two low-wave backscatter measurements are approximately the same, even though the sea temperature is different by more than a factor of two. Since all other conditions were basically the same, we conclude that the effects of sea temperature are negligible for these data sets.

Additionally, the air temperature is nearly constant, varying from $T_{\mathrm{air}} = 9.3$°C on Mar. 5, 1991 to $T_{\mathrm{air}} = 11.1$°C on Mar. 6, 1991. The atmosphere under these air and sea conditions is slightly unstable, and this instability increases with increasing sea temperature. Previous observations have shown an increase in the backscatter coefficient of the ocean surface with increasing atmospheric instability [24]. However, the atmospheric stability for these cases is small (z/L varies from -0.2 to -0.5), and the expected change in radar cross section is negligible. Reference [4] also predicts a difference of less than 1 dB per 10°C at these wind speeds (5 $\mathrm{m \cdot s^{-1}}$). Thus, the temperature difference would not cause a large backscatter difference in these cases.

ACKNOWLEDGMENT

The authors thank Dr. J. D. Oberholtzer and Dr. K. Steele for the buoy data, Dr. I. Popstefanija for additional C-SCAT data, and Dr. W. J. Plant for the ocean backscatter model.

REFERENCES

[1] W. L. Jones, L. C. Schroeder, D. H. Boggs, E. M. Bracalente, R. A. Brown *et al.*, "The SEASAT-A satellite scatterometer: The geophysical evaluation of remotely sensed wind vector over the ocean," *J. Geophys. Res.*, vol. 87, no. C5, pp. 3297–3317, 1982.

[2] E. P. W. Attema, "The active microwave instrument on-board the ERS-1 satellite," *Proc. IEEE*, vol. 79, 850–866, June 1991.

[3] S. L. Durden and J. F. Vesecky, "A physical radar cross-section model for a wind-driven sea with swell," *IEEE J. Ocean. Eng.*, vol. OE-10, no. 4, pp. 445–451, 1985.

[4] M. A. Donelan and W. J. Pierson, "Radar scattering and equilibrium ranges in wind-generated waves with application to scatterometry," *J. Geophys. Res.*, vol. 92, no. C5, pp. 4971–5029, 1987.

[5] W. J. Plant, "A two-scale model of short wind-generated waves and scatterometry," *J. Geophys. Res.*, vol. 91, no. C9, pp. 10735–10749, 1986.

[6] ——, "Correction to 'A two-scale model of short wind-generated waves and scatterometry,'" *J. Geophys. Res.*, vol. 93, no. C2, pp. 1347, 1988.

[7] W. C. Keller and W. J. Plant, "Cross sections and modulation transfer functions at L and Ku bands measured during the tower ocean wave and radar dependence experiment," *J. Geophys. Res.*, vol. 95, no. C9, pp. 16277–16289, 1990.

[8] F. Feindt, V. Wismann, W. Alpers, and W. C. Keller, "Airborne measurements of the ocean radar cross section at 5.3 GHz as a function of wind speed," *Radio Sci.*, vol. 21, no. 5, pp. 845–856, 1986.

[9] W. G. Large and S. Pond, "Open ocean momentum flux measurements in moderate to strong wind," *J. Phys. Oceanogr.*, vol. 11, 324–336, 1981.

[10] F. J. Wentz, S. Peteherych, and L. A. Thomas, "A model function for ocean radar cross sections at 14.6 GHz," *J. Geophys. Res.*, vol. 89, no. C3, pp. 3689–3704, 1984.

[11] F. J. Wentz, L. A. Mattox, and S. Peteherych, "New algorithms for microwave measurements of ocean winds: Applications to SEASAT and the special sensor microwave imager," *J. Geophys. Res.*, vol. 91, no. C2, pp. 2289–2307, 1986.

[12] A. E. Long, "C-band V-polarized radar sea echo model from ERS-1 Haltenbalken campaign," *URSI Microwave Signature Conf.* IGLS-Innsbruck, Austria, July 1–3, 1992.

[13] O. M. Phillips and M. L. Banner, "Wave breaking in the presence of wind drift and swell," *J. Fluid Mech.*, vol. 66, no. 4, pp. 625–640, 1974.

[14] O. M. Phillips, "Radar returns from the sea surface—Bragg scattering and breaking waves," *J. Phys. Oceanogr.*, vol. 18, 1065–1074, 1988.

[15] F. Li, W. Large, W Shaw, E. J. Walsh, and K. Davidson, "Ocean radar backscatter relationship with near-surface winds: A case study during FASINEX," *J. Phys. Oceanogr.*, vol. 19, no. 3, pp. 342–353, 1989.

[16] K. B. Katsaros, M. A. Donelan, and W. M. Drennan, "Flux measurements from a SWATH ship in SWADE," *J. Marine Syst.*, no. 4, pp. 117–132, 1993.

[17] D. E. Weissman, K. L. Davidson, R. A. Brown, C. A. Friehe, and F. Li, "The relationships between the microwave radar cross section and both wind speed and stress—Model function development using FASINEX data," *J. Geophys. Res.*, vol. 99, no. C5, pp. 10087–10108, 1994.

[18] L. C. Schroeder, D. H. Boggs, G. Dome, I. M. Halberstam, W. L. Jones *et al.*, "The relationship between wind vector and normalized radar cross section used to derive SEASAT-A satellite scatterometer winds," *J. Geophys. Res.*, vol. 87, no. C5, pp. 3318–3336, 1982.

[19] W. L. Jones, L. C. Schroeder, and J. L. Mitchell, "Aircraft measurements of microwave scattering signature of the ocean," *IEEE Trans. Antennas Propagat.*, vol. AP-25, pp. 52–61, Jan. 1977.

[20] H. Masuko, K. Okamoto, M. Shimada, and S. Niwa, "Measurement of microwave backscattering signatures of the ocean surfaces using X and K_a and Airborne Scatterometers," *J. Geophys. Res.*, vol. 91, no. C11, pp. 13065–13083, 1986.

[21] D. J. McLaughlin, R. E. McIntosh, A. Pazmany, L. Hevizi, and E. Boltniew, "A C-band scatterometer for remote sensing the air-sea interface," *IEEE Trans. Geosci. Remote Sens.*, vol. 29, pp. 260–267, Mar. 1991.

[22] F. K. Li, G. Neumann, S. Shaffer, and S. L. Durden, "Studies of the location of azimuth modulation for Ku band ocean radar backscatter," *J. Geophys. Res.*, vol. 93, no. C7, pp. 8229–8238, 1988.

[23] M. R. Keller, W. C. Keller, and W. J. Plant, "A wave tank study of the dependence of X band cross sections on wind speed and water temperature," *J. Geophys. Res.*, vol. 97, no. C4, pp. 5771–5792, 1992.

[24] W. C. Keller, W. J. Plant, and D. J. Weissman, "The dependence of X-band microwave sea return on atmospheric stability and sea state," *J. Geophys. Res.*, vol. 90, no. C1, pp. 1019–1029, 1985.

S. V. Nghiem (M'94) received the B.S. degree in electrical engineering from Texas A&M University at College Station, the M.S. and Ph.D. degrees from the Department of Electrical Engineering and Computer Science, Massachusetts Institute of Technology, Cambridge, in 1985, 1988, and 1991, respectivley.

In 1991, he joined the Jet Propulsion Laboratory, California Institute of Technology, Pasadena. His research includes electromagnetic wave theory and applications modeling of geophysical media, and polarimetric active and passive remote sensing.

Dr. Nghiem is a member of Phi Kappa Phi, and Sigma Xi.

Fuk K. Li (SM'89), for photograph and biography, please see p. 92 of the January issue of this TRANSACTIONS.

Shu-hsiang Lou was born in Seoul, Korea, in 1960. He received the B.S., M.S. and Ph.D. degrees in electrical engineering from the University of Washington, Seattle, in 1982, 1984 and 1991, respectively.

From 1985 to 1986, he worked in the area of fiber optics for the Eldec Sensing System Division in Bothell, WA. Since 1991, he has been working for the Jet Propulsion Laboratory, California Institute of Technology, Pasadena. He is a member of the technical staff in the Radar Science and Engineering section involving in the system design, analysis, and test of spaceborne scatterometers. His research interests include computational methods and numerical analysis, radar remote sensing, and applied electromagnetics.

Gregory Neumann was born in Ogden, Utah in 1956. He received the B.S. and M.S. degrees in electrical engineering from Brigham Young University, Provo, UT, in 1981 and 1984, respectively.

He has worked at the Jet Propulsion Laboratory, California Institute of Technology, Pasadena, since 1984 on airborne and spaceborne scatterometers.

Robert E. McIntosh (S'66–M'67–SM'72–F'85), for photograph and biography, please see p. 124 of the January issue of this TRANSACTIONS.

Steven C. Carson was born September 17, 1964, in Winterset. He received the B.Sc. degree in electrical engineering from Iowa State University, Ames, in 1988, and the Ph.D. degree in electrical engineering from the University of Massachusetts, Amherst in February 1993.

From June 1988 to December 1992, he was a Research Assistant at the Microwave Remote Sensing Laboratory, where he developed remote sensing radars, and studied radar backscatter from the ocean surface. In December 1992, he joined ARCO Power Technologies, Inc. in Washington, DC where he was an RF systems engineer. In January 1995, he joined American Electronics, Lanham, MD as a senior systems engineer. His current research interests include advanced radar, the design and development of RF and microwave instrumentation, and remote sensing.

James R. Carswell was born in Springifield, MA, in 1968. He received the B.S. degree in electrical engineering from Tufts University, Medford, MA, in 1990. He is pursuing the Ph.D. degree at the University of Massachusetts, Amherst.

Since 1990, he has been with the Microwave Remote Sensing Laboratory (MIRSL), ECE Department, University of Massachusetts. At MIRSL, he has designed and fabricated an airborne Ku-band scatterometer for investigating the backscatter from the ocean surface and its dependence upon environmental parameters, and has led the C-band scatterometer measurement campaigns during Hurricane Tina and the Tropical Ocean Global Atmosphere Coupled Ocean-Atmosphere Response Experiment. His current research is focussed on characterizing C-band backscatter measurements from the ocean surface under low-wind conditions.

Mr. Carswell is a member of American Geophysical Union, Tau Beta Pi, and Eta Kappa Nu.

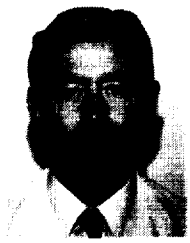

Edward J. Walsh (S'60–M'74) received the B.S. and Ph.D. degrees in electrical engineering from Northeastern University, Boston, MA, in 1963 and 1967, respectively.

From 1967 to 1970, he investigated MF ducted propagation in the Earth's magnetosphere at the NASA Electronics Research Center, Cambridge, MA, both as a civil servant and a military detailee (1968–1970) as a Signal Corps officer from the U.S. Army. Since 1970, he has been with the NASA GSFC Wallops Flight Facility in Wallops Island, VA. His research interests are in the general area of remote sensing and radio oceanography, using tower-based, airborne, and satellite systems. Particular areas include the measurement and interpretation of the ocean directional wave spectrum, the sea surface mean square slope, and the variation of sea surface radar cross section as a function of parameters such as incidence angle, sea surface slope, deviation from mean sea level, wind speed, and stress.

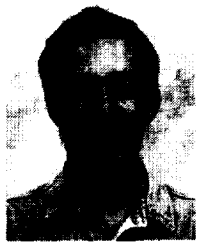

Mark A. Donelan received the B.Eng. degree in electrical engineering from McGill University, Montreal, PQ, Canada, and the Ph.D. degree in physics (oceanography) from the University of British Columbia, Vancouver, BC, Canada, in 1964 and 1970, respectively.

After a postdoctoral fellowship at the University of Cambridge, he joined the staff of the National Water Research Institute at the Canada Centre for Inland Waters, Burlington, Ontario. His research interests are in many aspects of air-sea interaction, primarily momentum, heat and mass transfer and the generation, propagation and dissipation of surface gravity waves.

William M. Drennan received the B.Sc. degree in mathematics and engineering from Queen's University, St. John's, NF, Canada, in 1982, and the Ph.D. degree in applied mathematics from the University of Waterloo, Waterloo, ON, Canada, in 1989.

His research interests include air-sea interaction, wave dynamics and techniques of analysis.